Characterization of Electrohydrodynamic Force on Dielectric-Barrier-Discharge Plasma Actuator Using Fluid Simulation

Hiroyuki Nishida, Taku Nonomura, and Takashi Abe

Abstract—Wall-surface jet induced by the dielectric barrier discharge (DBD) has been proposed as an actuator for active flow control in aerodynamic applications. Discharge plasma evolution of the DBD plasma actuator was simulated based on a simple fluid model, in which the electron, one type of positive ion and negative ion were taken into account. Two-dimensional simulation was conducted, and the results are in agreement with the insights obtained from experimental studies. The simulation results indicate that the discharge mode changes depending on applied voltage slope; when the applied voltage is positive-going with high applied voltage slope, the corona-type discharge mode turns into the streamer-type discharge mode and the threshold voltage slope is around 300 kV/ms in this simulation. The characteristics of the electrohydrodynamic (EHD) force, which is the source of the wall-surface jet, also change depending on the discharge mode; the tentative peak value of the EHD force during the positive-going voltage phase is saturated by the periodical formation of the streamer-type discharge.

Keywords—Dielectric barrier discharge, Plasma actuator, Fluid simulation.

I. Introduction

WALL-surface jet induced by the dielectric barrier discharge (DBD) has been proposed as actuators for flow control in aerodynamic applications[1]-[3]. A schematic diagram of a generic DBD plasma actuator is shown in Fig. 1. It consists of two electrodes separated by a dielectric and displaced in the streamwise direction. An alternating voltage with frequency of several kHz and amplitude of thousands of volts is applied to the exposed (top) electrode, and a dielectric barrier discharge appears from the exposed electrode edge; the wall-surface jet is induced as shown in Fig. 1. The DBD plasma actuator attached on an object surface can add the momentum to the boundary layer flow, and the flow separation can be controlled. This is expected to be a promising application of plasma physics to aerodynamic flow control due to its advantages over conventional devices; a very thin structure, light weight and no mechanical moving parts.

Many research efforts have been devoted to the feasibility study of the DBD plasma actuator for aerodynamic flow control , and significant flow control gains (drag reduction, improving stall characteristics and so on) have been observed in laboratory experiments under the condition of low Reynolds number (low free-stream speed) [1]-[3]. However, under the condition of high Reynolds number, the gains by the DBD plasma actuator drastically reduce due to its small momentum of the wall-surface jet compared to that of the free-stream [4]. The wall-surface jet strength has to be enhanced by two-orders of magnitude for real applications, and further intense studies are undergoing worldwide.

The momentum coupling between charged particles and neutral molecules of the ambient gas is the source of the electrohydrodynamic (EHD) force, which accelerates the ambient gas. Intense studies have been conducted to understand the detail mechanism of the momentum transfer process [5]-[23]; however, the understanding is only partial. Comprehensive understanding of the physics involved in the DBD plasma actuator is very significant to indicate the guidelines for the wall-surface jet enhancement. Although the experimental investigations [5]-[8], [13]-[17], [19] have provided many valuable insights into the physics of the DBD plasma actuator, it is difficult to experimentally measure detail plasma parameters. Numerical simulation of the discharge plasmas is an usable analytical tool for a comprehensive understanding of the physics, and a number of numerical model have been proposed for the DBD plasma actuator [9]-[12], [20]- [23].

In this study, a simple fluid model is adopted for numerical analysis, in which the electron, one type of positive ion and negative ion are taken into account, and the analysis focuses on the relation of the applied voltage slope to the characteristics of the discharge and EHD force.
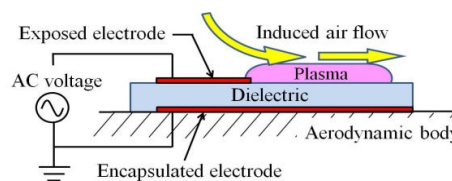
Hiroyuki Nishida is with Tokyo University of Agriculture and Technology, Koganei, 184-8588, Japan (phone: +81-42-388-7078; fax: +81-42-388-7078; e-mail: hnishida@cc.tuat.ac.jp).

Taku Nonomura is with Institute of Space and Astronautical Science, Japan Aerospace Exploration Agency, Sagamihara, 252-5210, Japan.

Takashi Abe is with Institute of Space and Astronautical Science, Japan Aerospace Exploration Agency, Sagamihara, 252-5210, Japan.

Fig. 1 Schematic of DBD plasma actuator

II. Numerical Model

A. Modeling of Discharge Plasma

The ambient gas is assumed to be the air. Detail plasma chemistry of the air is not considered in this study because the objective of our study is to understand the basic physics related to the EHD force production.

The numerical model is the same as that used in the references [10]-[11], [23]. We consider the electron, and one type of positive ion and one type of negative ion with a basic plasma chemistry including electron impact ionization ($N_2+e\rightarrow N_2^++e+e$), electron attachment ($O_2+e\rightarrow O+O^-$) and recombination. The time dependent electron and ions continuity equations with drift-diffusion fluxes are coupled with the Poisson's equation. The governing equations are as follows;

$$\frac{\partial n_e}{\partial t} + \nabla\cdot\left(-n_e\mu_e\mathbf{E} - D_e\nabla n_e\right) = (\alpha-\eta)n_e|v_e| - r_{ep}n_e n_p, \quad (1)$$

$$\frac{\partial n_p}{\partial t} + \nabla\cdot\left(n_p\mu_p\mathbf{E} - D_p\nabla n_p\right) = \alpha n_e|v_e| - r_{ep}n_e n_p - r_{pn}n_p n_n, \quad (2)$$

$$\frac{\partial n_n}{\partial t} + \nabla\cdot\left(-n_n\mu_n\mathbf{E} - D_n\nabla n_n\right) = \eta n_e|v_e| - r_{pn}n_p n_n, \quad (3)$$

$$\nabla\cdot\left(\varepsilon_r\mathbf{E}\right) = \frac{e}{\varepsilon_0}\left(n_p - n_e - n_n\right) + \frac{e}{\varepsilon_0}\sigma\delta_s. \quad (4)$$

Here, μ_k (with $k=e, p, n$; electron, positive ion, negative ion, respectively) and D_k are the charged particle mobility and the diffusion coefficient, respectively. α and η are the ionization and attachment coefficient, r_{ep} and r_{pn} are the electron-positive ion and positive-negative ion recombination coefficient, respectively. σ, in the Eq. (4), is the surface charge density, which is non-zero only on the dielectric surface, as expressed by the Dirac function δ_s. The surface charge density is calculated self-consistently by integrating the electron and ion fluxes to the surface. In the Eq. (4), ε_0 is the vacuum permittivity, and ε_r is the relative permittivity, which is equal to 5 inside of the dielectric layer.

These governing equations are calculated by the finite volume method. The drift terms in the equations (1), (2) and (3) are evaluated by the upwind scheme with the MUSCL interpolation, and the diffusion terms are evaluated by the central difference scheme. The time integration is conducted by the implicit scheme. The Poisson equation (4) is solved by the SOR method with the semi-implicit technique [9].

B. Computational Settings

A micro-discharge of the DBD plasma actuator is simulated in the two-dimensional space. The Computational settings are shown in Fig. 2. In the initial state, the simulation domain (air region) is filled with uniform density plasma ($n_e = n_p = 10^9$ m^{-3}). The alternating voltage is applied to the exposed electrode, and the potential of the bottom electrode is 0 V throughout the simulation. The boundary condition for the Poisson's equation is zero field perpendicular to the simulation domain boundary. The boundary condition for the charged particle at the left, right and top boundary is zero density gradients. The secondary electron emission under ion bombardment is considered as the boundary condition for the dielectric and electrode surface:

$$\mathbf{J}_{e,\perp} = \gamma\mathbf{J}_{i,\perp}, \quad (5)$$

where $\mathbf{J}_{e\perp}$ and $\mathbf{J}_{i\perp}$ are the components of the electron and ion current densities perpendicular to the surface, and γ is the secondary electron emission coefficient (=0.05).

The ionization and attachment coefficients, and the electron mobility are calculated by the BOLSIG software [24] assuming the ambient gas is the air (N_2:O_2=0.8:0.2). The recombination coefficients r_{ep} and r_{pn} are equal to 2×10^{-13} m^{3}s^{-1}. The positive and negative ion mobilties are set to be constant; $\mu_p = 21.0/p$ m^{2}V^{-1}s^{-1} and $\mu_n = 24.0/p$ m^{2}V^{-1}s^{-1}, where p is the ambient gas pressure (= 1×10^5 Pa). The diffusion coefficients are chosen so that $D_e / \mu_e = 1$V and $D_{p,n} / \mu_{p,n} = 0.01$V.

The computational domain is divided into uniform grid system; the grid size is 20 μm.
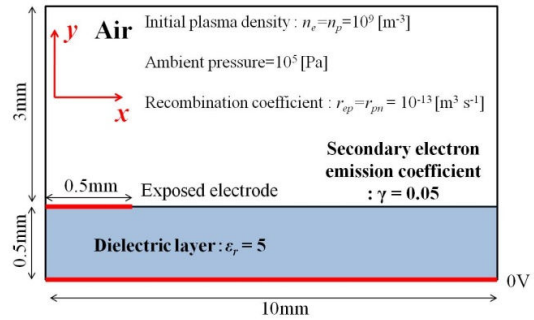

Fig. 2 Computational settings

C. EHD Force

The EHD force per unit volume is due to the momentum transfer from charged particles to neutral particles. The EHD force, $\mathbf{F}$, in collisional plasma can be obtained assuming that the force is equal to the rate of momentum transfer per unit volume due to collisions [8]-[11].

$$\mathbf{F} = \frac{\mathbf{J}_p}{\mu_i} - \frac{\mathbf{J}_e}{\mu_e} - \frac{\mathbf{J}_n}{\mu_n} = e\left(n_p - n_e - n_n\right)\mathbf{E} - \left[\frac{D_p}{\mu_p}\nabla n_p + \frac{D_e}{\mu_e}\nabla n_e \frac{D_n}{\mu_n}\nabla n_n\right]. \quad (6)$$

III. RESULTS AND DISCUSSION

A. Validity of the Simulation Model

In this section, the validity of the numerical simulation is briefly mentioned.

Precise experimental studies have been conducted by many researchers to clarify the performance characteristics of the DBD plasma actuator [5]-[8], [13]-[17], [19], and one of the important benchmark of the performance is thrust force, which is the reaction force acting on the DBD plasma actuator due to producing the jet. In the numerical simulation, the space integrated and time averaged EHD force is used for the comparison with the experiment. Note that a part of the EHD force is lost due to the friction force between the wall-surface jet and the dielectric surface; therefore the qualitative comparison is conducted.

The simulation is conducted for the sinusoidal applied voltage waveform. Figure 3 shows the (integrated and averaged) EHD force as a function of the applied voltage amplitude with a constant frequency of 10 kHz. In Fig. 4, the EHD force is plotted as a function of the frequency with constant voltage amplitude of 15 kV. The characteristics of the

EHD force shown in Figs. 3 and 4 are consistent with the knowledge obtained by the previous experimental researches. More detail validation study of the numerical model is shown in the references [22]-[23]. As described above, the numerical model adopted in this study can successfully simulate the characteristics of the DBD plasma actuator in many aspects, which are consistent with the experiment. Therefore, valuable insights into the physics of DBD plasma actuator are expected to be obtained from this numerical model and its simulation results.
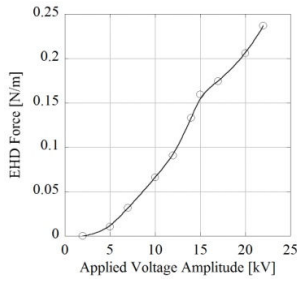
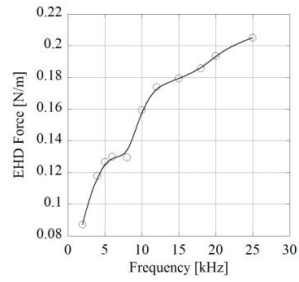Fig. 3 Voltage characteristics of the EHD force

Fig. 4 Frequency characteristics of the EHD force

B. Discharge Mode

The simulation results show that the discharge state changes depending on the applied voltage amplitude and the frequency.

The applied voltage waveform and the discharge current waveform are plotted in Figs. 5 (a) and (b) for low (7 kV$_{peak}$) and high (20 kV$_{peak}$) applied voltage amplitude with a constant frequency (10 kHz), respectively. During the negative-going voltage phase, the negative current spike appears with high frequency. Although the peak value and the generation frequency of the current spike become lower with lower applied voltage amplitude, large difference in the discharge characteristics cannot be observed. Figure 6 shows the typical discharge plasma structure during the negative-going voltage phase (the voltage amplitude of 15 kV$_{peak}$ and the frequency of 10 kHz); the electric potential and positive ion density distributions are plotted. The discharge mode during the negative-going voltage phase is categorized into the glow-type discharge. On the other hand, during the positive-going voltage phase, the discharge state at the high applied voltage significantly changes from that at the low applied voltage; large positive current spike periodically appears at the high applied voltage. The discharge plasma structure with the low applied voltage at t = 0.2014 ms and t = 0.2243 ms are shown in Figures 7(a) and (b), respectively. The discharge plasma is ignited near the exposed electrode edge, and gradually expands along the dielectric surface; this discharge type is the corona-type discharge. In the case of the high applied voltage amplitude, the discharge mode transition occurs as shown in Fig. 8; during the first stage, the corona-type discharge appears near the exposed electrode edge (see Fig. 8(a) at t = 0.2019 ms), and after that, the discharge mode is transit to the streamer-type discharge (see Fig. 8(b) at t = 0.2041 ms), in which a high-density plasma column propagates from the exposed electrode edge along the dielectric surface. The generation of the streamer-type

discharge corresponds to the appearance of the positive current spike.
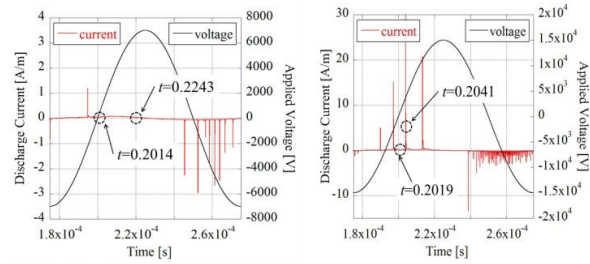

(a) 7 kV$_{peak}$ (b) 15 kV$_{peak}$

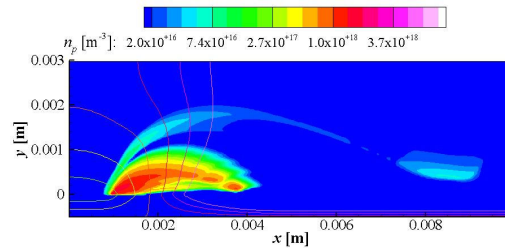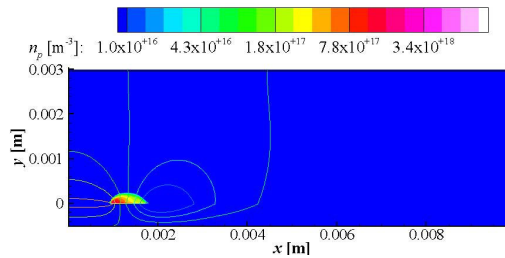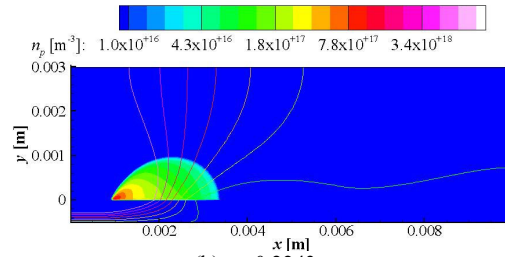Fig. 5 Applied voltage and discharge current waveform with a frequency of 10 kHz

Fig. 6 Typical plasma structure during the negative-going voltage phase; the positive ion distributions and the electric potential distributions

(a) t = 0.2014 s

(b) t = 0.2243 s

Fig. 7 Discharge plasma structure during the positive-going voltage phase at the low applied voltage amplitude; 7 kV$_{peak}$ 10 kHz

The applied voltage and the discharge current waveform for low (4 kHz) and high frequency (20 kHz) with constant voltage (15 kV) are plotted in Fig. 9(a) and (b), respectively. During the negative going voltage phase, large difference is not observed in the discharge characteristics at between the low and high frequency. On the other hand, during the positive-going voltage phase, the discharge mode transition from the corona-type

discharge to the streamer-type discharge can be observed. The discharge mode transition with an increase in the frequency is similar to that with an increase in the applied voltage amplitude; this result indicates that the applied voltage slope (dV/dt) decides whether the discharge mode transition occurs or not. The threshold voltage slope is about 300 kV/ms in this simulation.
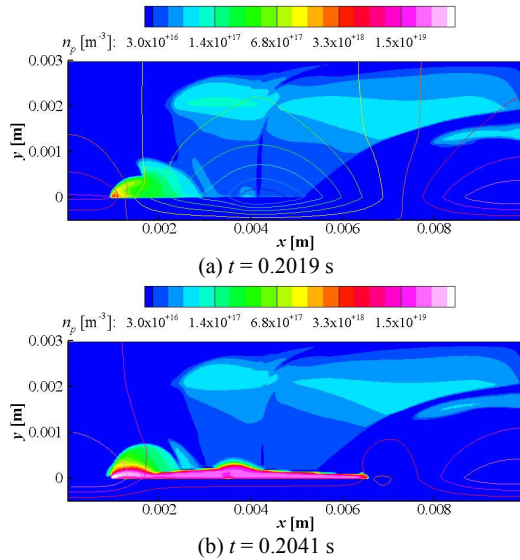

(a) $t = 0.2019$ s

(b) $t = 0.2041$ s

Fig. 8 Discharge plasma structure during the positive-going voltage phase at the high applied voltage amplitude; 15 kV$_{peak}$ 10 kHz
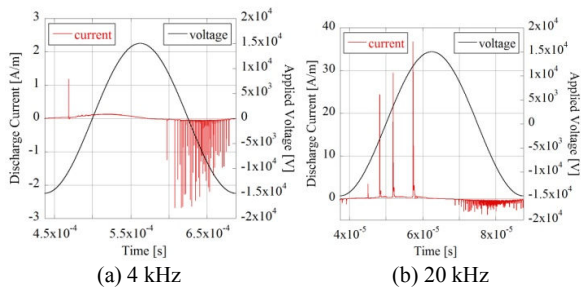

(a) 4 kHz   (b) 20 kHz

Fig. 9 Applied voltage and discharge current waveform with an applied voltage amplitude of 15 kV

C. EHD Force

The characteristics of the EHD force are shown for the each discharge mode. Figure 10(a) and (b) shows the time history of the space-integrated EHD force in the case of the corona-type discharge (the peak voltage of 7 kV and the frequency 10 kHz; low voltage slope) and the streamer-type discharge (the peak voltage of 15 kV and the frequency 10 kHz; high voltage slope), respectively. During the negative-going voltage phase, the EHD force increases with time until the applied voltage reaches the negative peak value, and after that, the EHD force rapidly reduces until the positive-phase discharge starts; the characteristics is the same in both voltage slope cases. On the other hand, during the positive-going voltage phase, the EHD force characteristics are totally different between the two voltage slope cases. In the case of the low voltage slope (the

corona-type discharge), the EHD force increases with time until the applied voltage reaches the positive peak value. However, in the case of the high voltage slope (the streamer-type discharge), the increment of the EHD force is disrupted by the formation of the streamer discharge, and as a result, the tentative amplitude of the EHD force is saturated (it was shown also by Boeuf et al. [10] that the EHD force generation is disrupted by the streamer discharge).

The parameter characteristics of the time-averaged EHD force is also strongly affected by the discharge mode. One example is shown here. Figure 11 shows the time-averaged (and the space-integrated) EHD force for three types of the saw tooth applied voltage waveform; Fig. 11(a) shows the case of the low (the peak voltage of 15 kV and the frequency 10 kHz), and (b) shows the high voltage slope case (the peak voltage of 20 kV and the frequency 10 kHz). As shown in Fig. 11, the EHD force magnitude relation between the waveform 1 and 3 (see Fig. 11) is reversed between the low and the high voltage slope case. The waveform characteristics of the EHD force at the high voltage slope (Fig. 11(b)) have been experimentally observed in the condition of much lower voltage slope (less than 8×10^4 kV/s) [13], and this result implies that the discharge mode tends to transit to the streamer-type discharge mode. This is because three-dimensional small disturbances in the electrode shape and the atmosphere condition encourage the electric field concentration.
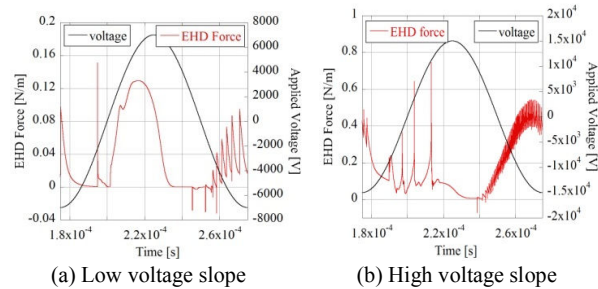

(a) Low voltage slope   (b) High voltage slope

Fig. 10 Time history of the space integrated EHD force in the case of the low voltage slope and the high voltage slope

IV. Conclusion

The discharge plasma evolution of the DBD plasma actuator, which is an active flow control device, was simulated using the plasma fluid model. The electron, one type of positive ion and negative ion are taken into account, and the validity of the numerical model has been shown by the comparison with the experimental results. The simulation results indicate that the discharge characteristics during the negative going voltage phase does not depend on the applied voltage amplitude and the frequency. On the other hand, the discharge mode during the positive-going voltage phase changes depending on the applied voltage slope; although only the corona-type discharge appears in the case of the low voltage slope, the discharge mode transition from the corona-type discharge to the streamer-type discharge occurs at the higher voltage slope than about 300 kV/ms. The characteristics of the electrohydrodynamic force, which is the source of the wall-surface jet, also change

depending on the discharge mode; the tentative peak value of the EHD force during the positive-going voltage phase is saturated by the periodical formation of the streamer-type discharge.

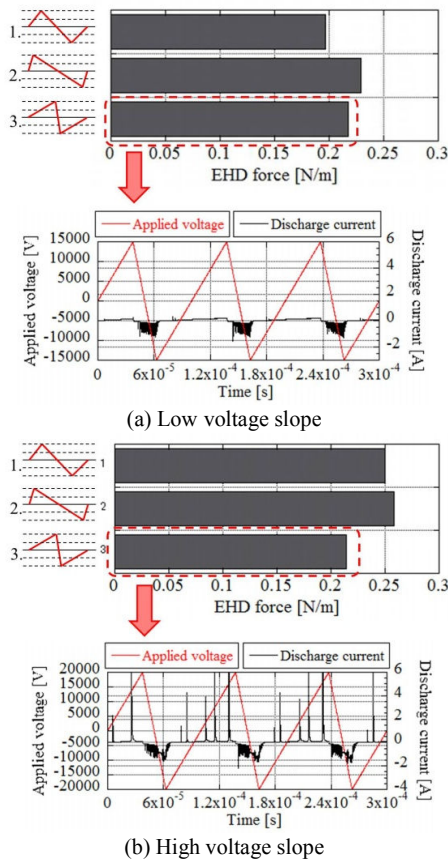(a) Low voltage slope

(b) High voltage slope

Fig. 11 The waveform characteristics of the space integrated and time averaged EHD force; lower-half figure in (a) and (b) shows the applied voltage and discharge current waveform

REFERENCES

[1] J. R. Roth , D. M. Sherman, and S. P. Wilkinson, "Electrohydrodynamic Flow Control with a Glow-Discharge Surface Plasma",*AIAA J.*, vol. 38, 2000, pp. 1166-1172.
[2] M. L. Post and T. C. Corke, "Separation Control on High Angle of Attack Airfoil using Plasma Actuator",*AIAA J.,* vol. 42, 2004, pp. 2177-2184.
[3] M. L. Post and T. C. Corke, "Separation Control using Plasma Actuators: Dynamic Stall Vortex Control on Oscillating Airfoil",*AIAA J.,* vol. 44, 2006, p. 3125-3135.
[4] T. Matsuno, K. Ota, T. Kanatani and H. Kawazoe, "Development of Trielectrode Plasma Actuator and Its Application to Delta Wing Vortex Control," *29th AIAA Applied Aerodynamics Conf.*, Honolulu, 2011, AIAA 2011-3514.
[5] C. L. Enloe, R. D. McLaughlin, G. I. Font and J. W. Boughn, "Parameterization of Temporal Structure in the Single-Dielectric-Barrier Aerodynamic Plasma Actuator," *AIAA J.*, Vol. 44, 2006, pp. 1127-1136.
[6] C. O. Porter, J. W. Baughn, T. E. McLaughlin, C. L. Enloe and G. I. Font, "Plasma Actuator Force Measurement," *AIAA J.*, Vol. 45, 2007, pp. 1562-1570.
[7] C. L. Enloe, G. I. Font, T. E. McLaughlin and D. M. Orlov, "Surface Potential and Longitudinal Electric Field Measurements in the Aerodynamics Plasma Actuator," *AIAA J.,* Vol. 46, 2008, pp. 2730-2740.
[8] C. Porter, A. Abbas, K. Cohen, T. McLaughlin and C. L. Enloe, "Spatially Distributed Forcing and Jet Vectoring with a Plasma Actuator," *AIAA J.*, Vol. 47, 2009, pp. 1368-1378.
[9] J. P. Boeuf and L. C. Pitchford, "Electrohydrodynamic force and aerodynamic flow acceleration in surface dielectric barrier discharge", *J. of Applied Physics,* Vol. 97, 2005, pp. 103307-1 – 103307-10.
[10] J. P. Boeuf, T. Lagmich, Th. Unfer, Th. Callegari and L. C. Pitchford, "Electrohydrodynamic Force in Dielectric Barrier Discharge Plasma Actuators", *J. of Physics D: Applied Physics*, vol. 40, 2007, pp. 652-662.
[11] Y. Lagmich, Th. Callegari, L. C. Pitchford and J. P. Boeuf, "Model Description of Surface Dielectric Barrier Discharges for Flow Control",*J. of Physics D: Applied Physics*, vol. 41, 2008, pp. 095205-1 - 095205-10.
[12] A. V. Likhanskii, V. Semak, D. Opaits, M. Shneider, R. Miles and S. Macheret, "The role of the photoionization in the numerical modeling of the DBD plasma actuator", *47th AIAA Aerospace Science Meeting*, 2009, AIAA 2009-841.
[13] N. Kimura, S. Sato, T. Abe and Y. Takizawa, "A Parametric Experimental Study for Momentum Transfer by Plasma Actuator", *45th AIAA Aerospace Science Meeting*, Reno, 2007, AIAA 2007-187.
[14] Y. Takizawa, A. Matsuda, K. Kikuchi, T. Abe and A. Sasoh, "Optical Observation of Discharge Plasma Structure in DBD Plasma Actuator", *38th AIAA Plasmadynamics and Lasers Conf.*, Miami, 2007, AIAA 2007-4376.
[15] T. Abe, Y. Takizawa, S. Sato and N. Kimura, "Experimental Study for Momentum Transfer in a Dielectric Barrier Discharge Plasma Actuator", *AIAA J.*, Vol. 46, 2008, pp. 2248-2256.
[16] T. Abe and M. Takagaki, "Momentum Coupling and Flow Induction in a DBD Plasma Actuator", *40th AIAA Plasmadynamics and Lasers Conf.*, San Antonio, 2009, AIAA 2009-4068.
[17] C. L. Enloe, M. G. McHarg, G. I. Font and T. E. McLaughlin, "Plasma-induced force and self-induced drag in the dielectric barrier discharge aerodynamic plasma actuator", *47th AIAA Aerospace Science Meeting*, Reno, 2009, AIAA 2009-1622.
[18] G. I. Font, C. L. Enloe and T. McLaughlin, "Effects of Volumetric Momentum Addition on the Total Force production of a Plasma Actuator", *39th AIAA Fluid Dynamics Conf.*, San Antonio, 2009, AIAA 2009-4285.
[19] C. L. Enloe, G. I. Font, J. Newcomb, A. Teague, A. Vasso and T. McLaughlin, "Effects of Oxygen Content on the Behavior of the Dielectric Barrier Discharge Aerodynamic Plasma Actuator", *48th Aerospace Science Meeting*, Orland, AIAA 2010-545.
[20] D. M. Orlov, G. I. Font and D. Edelstein, "Characterization of Discharge modes of Plasma Actuators", *AIAA J.*, vol. 46, 2008, pp. 314-3148.
[21] J. Poggie, "High-Order Numerical Methods for Electrical Discharge modeling", *41st AIAA Plasmadynamics and Lasers Conf.*, Chicago, 2010, AIAA 2010-4632.
[22] H. Nishida and T. Abe, "Numerical analysis of plasma evolution on dielectric barrier discharge plasma actuator," *J. of Applied Plasma Physics*, vol. 110, 2011, pp. 013302-1 – 013302-9.
[23] H. Nishida and T. Abe, "Validation Study of Numerical Simulation of Discharge Plasma on DBD Plasma Actuator," *42nd AIAA Plasmadynamics and Lasers Conf.*, Honolulu, 2011, AIAA 2011-3913.
[24] See http://www.siglo-kinema.com/bolsig.htm for more information about the Bolsig database.